



Preparation and characterization of polyacrylonitrile nanofiber adsorbent modified with 6-amino-1-hexanethiol hydrochloride for the adsorption of thorium (IV) ion from aqueous solution

B. Rouhi Broujeni^{a,*}, A. Nilchi^b

^aDepartment of Natural Resources and Environment, Tehran Science and Research Branch, Islamic Azad University, PO Box 1478814656, Tehran, Iran, Tel. +98-9177200822; email: babak.rouhi@srbiau.ac.ir

^bMaterials and Nuclear Fuel Research School, Nuclear Science and Technology Research Institute, PO Box 11365-8486, Tehran, Iran, email: anilchi@aeoi.org.ir

Received 10 March 2018; Accepted 18 August 2018

ABSTRACT

In this study, novel polyacrylonitrile (PAN) nanofiber adsorbent modified with 6-amino-1-hexanethiol hydrochloride (Ahh) was synthesized by electrospinning method and evaluated as an adsorbent for removing thorium (IV) (Th^{4+}) ion from aqueous solution. The PAN/Ahh was characterized by X-ray diffraction (XRD), Fourier-transform infrared (FT-IR), scanning electron microscopy (SEM), and Brunauer–Emmett–Teller (BET). Response surface methodology (RSM) was utilized in the optimization of Th^{4+} adsorption in terms of (i.e., initial Ahh concentration, pH, the initial metal ion concentration, and contact time). To ensure the validity of the model, the statistical measures were investigated, thus to specify that the developed model is proper. In addition, the adsorption kinetics was well defined by the pseudo-second-order equation, while the Langmuir model better fit the adsorption isotherms. The adsorption capacity of PAN/Ahh was $499 \text{ mg Th}^{4+} \text{ g}^{-1}$ composite, leads to 98.5% removal at 25°C . Moreover, thermodynamic parameters were determined which point out the natural and endothermic nature of the reactions. The loaded Th^{4+} can be easily regenerated with HNO_3/HCl and the PAN/Ahh could be used repeatedly without any significant reduction in its adsorption capacity. The desorption level of Th^{4+} from the PAN/Ahh was more than 94%.

Keywords: PAN nanofiber; 6-amino-1-hexanethiol hydrochloride; Electrospinning; Adsorption; Th^{4+}

1. Introduction

Liquid processes and waste streams at nuclear facilities in the whole world have led to increase in production of radioactive contaminants waste and consequently the arrival of toxic and hazardous ions to the environment [1]. These ions have high toxicity even in very low concentrations and are extremely harmful for the environment and health [2]. One of the major radioactive ions that are very useful as a nuclear fuel and is found in wastewaters resulting from the production of nuclear fuels is Th^{4+} , which can be used as nuclear fuel by conversion into uranium-233

(^{233}U) [3,4]. Soil, rocks, sand, and water are the main source of thorium and because its availability is three to four times higher than uranium, this ion has attracted a lot of interest as a nuclear fuel [5,6]. In addition, in the cycle of using thorium as the primary fuel, the raw material is less used and consequently, the waste produced is less too [5]. Moreover, other thorium compounds and alloys have various applications; for example, thorium is used in high-quality lenses or the manufacture of ceramics at high temperatures [7]. Therefore, regarding the wide usage of thorium in industries and its long-term stability in the environment, as well as its potential harm to human well-being and the environment, the exclusion and recovery of this ion from wastewaters are required [8].

* Corresponding author.

Various techniques have been utilized for the recovery of thorium from waste comprising this ion. Some of these methods are solvent extraction, chemical precipitation, ion exchange, evaporation, biosorption, and adsorption [9–15]. For example, a combination of chemical precipitation and filtration in a series of sand-beds was used to remove radionuclides from waterworks effluent [16]. Chen et al. [17] employed silica-based anion exchange resins in order to remove thorium from nitric acid solutions. Li et al. [18] separated the Th^{4+} from sulfuric and phosphoric acid solutions by solvent extraction method. Many of these methods can be criticized from different points of view such as the economic, health, and production of hazardous wastes [19]. Amongst the reported techniques, adsorption is one of the most accepted methods of removing heavy metals from aqueous solutions, due to its features such as high efficiency, low cost, easy reduction, and lack of sludge production [20].

One of the favorable organic binder's polymer adsorbent is polyacrylonitrile (PAN). PAN is a synthetic, semicrystalline organic polymer resin, with the linear formula $(\text{C}_3\text{H}_3\text{N})_n$, which can be attained from blends of monomers with acrylonitrile as the main component [21]. All polymeric adsorbents have some weak points such as softness, tendency to agglomerate or form gels, low porosity, low surface area, hydrodynamic limitations in adsorption column, and nonavailability of reactive binding sites [22,23]. In this context, recent research has inclined to modify and combine PAN with other adsorbents [24–26]. There are a number of researches on the adsorption of radioactive ions by PAN and its derivatives, but only few papers are available on the usage of modified PAN-based nanofiber. For example, PAN-TiO₂ nanofiber adsorbent modified with aminopropyltriethoxysilane was reported to adsorb radioactive thorium ions [27]. In a similar study, the adsorption of thorium and uranyl ions by modified PAN composite nanofiber adsorbent has been reported [28].

In this study, the novel PAN/Ahh nanofibers were synthesized via electrospinning method. X-ray diffraction (XRD), Fourier-transform infrared (FT-IR), and scanning electron microscopy (SEM) characterized the structure of PAN/Ahh and its adsorption properties for the removal of Th^{4+} under varied experimental situations were considered. The adsorptive characteristics were evaluated based on adsorption parameters received from the adaptability of adsorption isotherms to the Langmuir and Freundlich models. In addition, kinetic data have modeled by the pseudo-first and second-order kinetic models. All the experiments and analyses were accomplished in laboratories of nuclear science and technology research institute of Iran.

2. Experimental

2.1. Materials and method

All the chosen reagents were of analytical grade and purchased from Merck (Germany), excluding PAN with molecular weight = 150,000, which was obtained from Aldrich (Poole, UK). The stock solutions for preparation of Th^{4+} were provided by dissolving thorium salt ($\text{Th}(\text{NO}_3)_4 \cdot 5\text{H}_2\text{O}$) in deionized water. The initial pH of solutions was regulated by nitric acid (HNO_3 ; 99.9%) or sodium hydroxide (NaOH ; 99.9%) solutions and Metrohm pH

meter model 744. Sartorius Electrical Balance Model BP 221S, Nabertherm furnace, and mixer HT Infors AG model CH-4103-BOT were applied to manage the experiments. The electrospinning system was employed to fabricate the PAN/Ahh nanofibers. The ultrasonic device was applied to homogenize the PAN polymer solution. Phase identification, crystallite size, and the composition of the PAN/Ahh were characterized by XRD obtained on Philips Xpert diffractometer using a scan speed of 0.015 S^{-1} and $\text{CuK}\alpha$ line ($\lambda = 1.5405 \text{ \AA}$) radiation with voltage and current of 40 kV and 40 mA, respectively. SEM (Cambridge S-360) considered morphological analysis and surface condition of the PAN/Ahh. Qualitative chemical structure evaluation was carried out via FTIR analysis (Vector22 Bruker Company, USA). Moreover, Brunauer-Emmett-Teller (BET) specific surface area was measured using a conventional BET multipoint N_2 physisorption apparatus utilizing Quantachrome NOVA 2200e system. The N_2 adsorption was measured from a six-point isotherm in a relative pressure range of 0.05–0.3 at 77.3K. The assumption for the cross-sectional area of N_2 was taken to be $16.2(\text{\AA})^2$ and the density used was 3.65 g cm^{-3} . The sample was degassed at 150°C for 2 h prior to BET analyses. Th^{4+} analysis was followed up by utilizing a Perkin-Elmer Optima 2000 DV model inductively coupled plasma-optic emission spectrometry (ICP-AES, Thermo Jarrel Ash, model Trace Scan). All the experimental data were the averages of the duplicate experiment, and the average relative error was smaller than 5%.

2.2. Synthesis of PAN/Ahh

PAN nanofibers were modified by the 6-amino-1-hexanethiol hydrochloride functional group to increase the adsorption capacity and to grow the active sites. For this purpose, different amounts of Ahh (based on PAN) were dissolved in 20 mL of dimethyl sulfoxide solution at a temperature of 60°C and stirred for 12 h. Finally, the solution was added to 5 wt% of PAN solution and mixed for 2 h. Then, the PAN/Ahh nanofibers were synthesized by electrospinning. The voltage, drum speed, distance within the drum, the needle, and the polymer rate were 21 kV, 500 rpm, 80 mm, and 2.5 mL h^{-1} , respectively. Fig. 1 shows the reaction of dimethyl sulfoxide with 6-amino-1-hexanethiol hydrochloride functional and PAN nitrile group.

2.3. Adsorption experiments

Batch experiments were considered to study the extent of Th^{4+} adsorption by PAN/Ahh in a polyethylene tube. The solution containing of Th^{4+} ion ($10\text{--}100 \text{ mg L}^{-1}$) was mixed with 0.2 g of the adsorbent at contact time (20–80 min), amine groups (5–55 wt% of Ahh with respect to the PAN weight) and pH values (2.0–8.0). The tube was placed in a

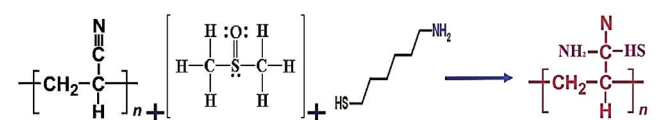


Fig. 1. Reaction of dimethyl sulfoxide with Ahh functional and PAN nitrile group.

thermostated shaker at 150 rpm. The initial pH of the Th⁴⁺ solutions was adjusted by adding 0.01 M HNO₃ or NaOH solutions. Following the adsorption procedure, the PAN/Ahh was separated by filtration and the residual concentration of the Th⁴⁺ ion was determined. In order to explore thermodynamic parameters, experiments were conducted at the optimized value of variables at five different temperatures (25°C, 30°C, 35°C, 40°C, and 45°C). The adsorption percentage (Ads%) and the amount of metal ion sorbed at time *t* (*q_e* and *q_t* mg g⁻¹) were calculated using Eqs. (1) and (2) as follows:

$$\text{Ads\%} = \frac{C_0 - C_e}{C_0} \times 100 \quad (1)$$

$$q_e = \frac{C_0 - C_e}{m} \times V, q_t = \frac{C_0 - C_t}{m} \times V \quad (2)$$

where *C₀* is the initial metal ion concentration (mg L⁻¹); *C_e* is the amount of metal present in the solution at equilibrium (mg L⁻¹); *V* is the volume of thorium solution (L); and “*m*” is the dry weight of the sample (g).

The adsorption process represented by the ion distribution coefficient, *K_d* (mL g⁻¹), was calculated using Eq. (3) as follows:

$$K_d = \frac{C_0 - C_e}{C_e} \times \frac{V}{m} \quad (3)$$

2.4. Experimental design for optimization

Central composite design was employed in the experimental design procedure consisting of 2^{*k*} factorial points (*k* = independent process variables), 2*k* axial points (*α* = 2) and six replicates at the center point to provide an estimate of the experimental error variance [29]. The Th⁴⁺ Ads% was selected as the response, while the pH, Th⁴⁺, and Ahh concentration and contact time were selected as decision variables. As a result, 30 experiments were conducted. The exact amounts of the coded levels for the variables are shown in Table 1.

A quadratic polynomial equation was considered to develop the relationship between the decision variables (*x*) and the response (*y*) using Eq. (4) as follows:

$$y = f(x)\beta_0 + \sum_{i=1}^k \beta_i x_i + \sum_{i=1}^k \sum_{j=i+1}^k \beta_{ij} x_i x_j + \sum_{i=1}^k \beta_{ii} x_i^2 + \varepsilon \quad (4)$$

where, *y* is response (dependent variable); β₀ is constant coefficient and β_{*i*}, β_{*ij*} and β_{*ii*} are coefficients for the linear, quadratic, and interaction effect, respectively; *x_i* and *x_j* are independent variables; and ε is the error of prediction.

The sequence of experimental runs, regression, and graphical analyses of the data was prepared by employing the Design Expert (version 7.0.0, Stat Ease, Inc., USA). The variability in the dependent variable (*y*) was explained and verified employing the coefficient of determination (*R*²) and adjusted *R*² (*R*²_{adj}), using Eqs. (5) and (6) as follows:

$$R^2 = 1 - \frac{SS_{\text{residual}}}{SS_{\text{model}} + SS_{\text{residual}}} \quad (5)$$

$$R^2_{\text{adj}} = 1 - \frac{n-1}{n-p} (1 - R^2) \quad (6)$$

where SS is the sum of the squares; *n* is the number of experiments; and *p* is the number of predictors (term) in the model [30]. The model equation was utilized to predict the optimum value of the variables leading to maximum removal percentage.

2.5. Desorption experiments

Desorption experiments were investigated in batch system using 0.1 M aqueous solutions of different reagents such as NaOH, NaCl, HCl, HNO₃, NaOH/NaCl, and HNO₃/HCl. The PAN/Ahh was placed in contact with the desorption solution for 24 h. The amount of Th⁴⁺ ion released into the solution was measured by the ICP spectrophotometric method. The Th⁴⁺ recovery percentage upon desorption from the PAN/Ahh was calculated using Eq. (7) as follows:

$$\text{Desorbed(\%)} = \left(1 - \frac{\text{Th}_{\text{ads}}^{4+} - \text{Th}_{\text{des}}^{4+}}{\text{Th}_{\text{ads}}^{4+}} \right) \times 100 \quad (7)$$

where Th⁴⁺_{ads} is the amount of adsorbed Th⁴⁺ (mg g⁻¹) and Th⁴⁺_{des} is the amount of desorbed Th⁴⁺ (mg g⁻¹).

The reusability was investigated by repeating the adsorption–desorption round up to five times and thus examine the long-term adsorption potential of PAN/Ahh.

3. Results and discussion

3.1. Characterization of PAN/Ahh

Fig. 2 illustrates XRD patterns of PAN and PAN/Ahh. The XRD pattern of PAN represents broad diffraction peaks

Table 1
Experimental factor levels for independent variables

Variables	Factor	Real values of coded levels		
		Low level (-1)	Center level (0)	High level (+1)
pH	A	3.5	5.0	6.5
Th ⁴⁺ concentration (mg L ⁻¹)	B	32.5	55	77.5
Contact time (min)	C	35	50.0	65
Ahh concentration (wt%)	D	17.5	30	42.5

at 20–17° and 29.3°, which are common fingerprints of crystal PAN [31]. It was also observed that the 2 γ values at the peak points of PAN/Ahh are the same as those in PAN. Thus, their structure is very similar.

The structure of PAN and PAN/Ahh was confirmed by FTIR analysis (Fig. 3). The spectra of PAN showed a broad adsorbance at 3,479–2,984 cm⁻¹ (combined peaks of the NH₂, hydroxyls, and OH group stretching vibration),

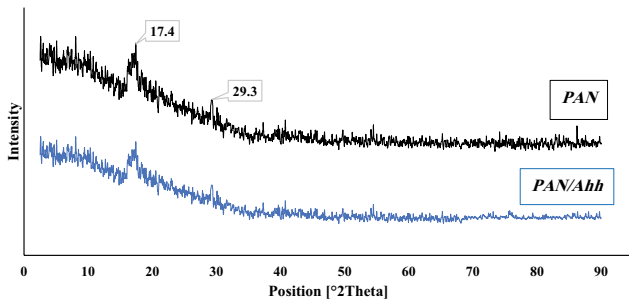


Fig. 2. XRD patterns of PAN and PAN/Ahh.

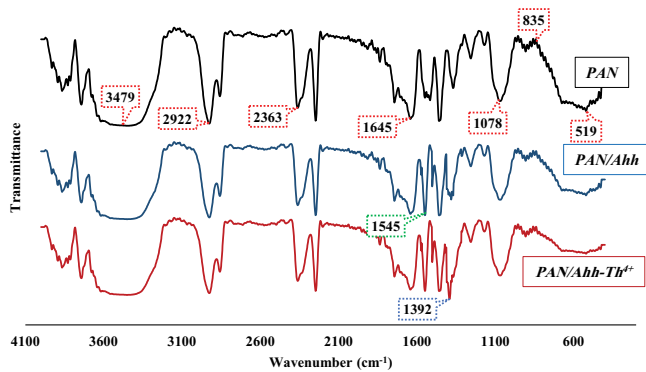


Fig. 3. FTIR spectra PAN, PAN/Ahh, and PAN/Ahh-Th⁴⁺.

at 2,922 and 2,363 cm⁻¹ (CH₃ and CH₂ in PAN structure), at 1,645–1,078 cm⁻¹ (attributed to the CONH₂ group), at 835 and 519 cm⁻¹ (CH bending of amide bonds stretching vibrations) [32]. In the PAN/Ahh curve, the banding vibration around 1,545 cm⁻¹ confirms the amine groups (N–H) have been successfully appended to the PAN nanofiber adsorbent [33]. After sorption of Th⁴⁺ ions, a new band characteristic for the identification of these ions with hydroxyl and amine groups becomes visible at 1,392 cm⁻¹ (in PAN/Ahh-Th⁴⁺ curve) [34].

The nitrogen adsorption and desorption studies showed that the BET surface area of PAN/Ahh site was 26.48 m² g⁻¹.

The SEM image and distribution diameter of PAN/Ahh nanofiber adsorbent are shown in Fig. 4. As shown in Fig. 4, the surface of PAN/Ahh nanofibers is smooth and the average diameter of nanofibers was about less than 100 nm [35]. Fig. 4 also shows that the morphology of nanofibers was virtually unchanged after coating Ahh functional group.

3.2. Model fitting

Thirty runs were conducted to compute the model and cover all the possible combinations of factor levels. The order of experiments and their results are shown in Table 2. A quadratic regression model was reached by employing coded values, as shown in Eq. (8) as follows:

$$\begin{aligned} \text{Ads}(\%) = & 97.46 + (0.28 \times A) - (2.30 \times B) - (0.81 \times C) + \\ & (1.49 \times D) - (1.08 \times A \times B) + (0.11 \times A \times C) + (0.39 \times A \times D) + \\ & (1.02 \times B \times C) - (1.40 \times B \times D) + (0.94 \times C \times D) - (2.94 \times A^2) - \\ & (1.6 \times B^2) + (0.47 \times C^2) - (1.68 \times D^2) \end{aligned} \quad (8)$$

The ANOVA estimates the validation of the model (Table 3). The small value of probability (Prob. > F; less than 0.05) proved the significance of the model [36]; while

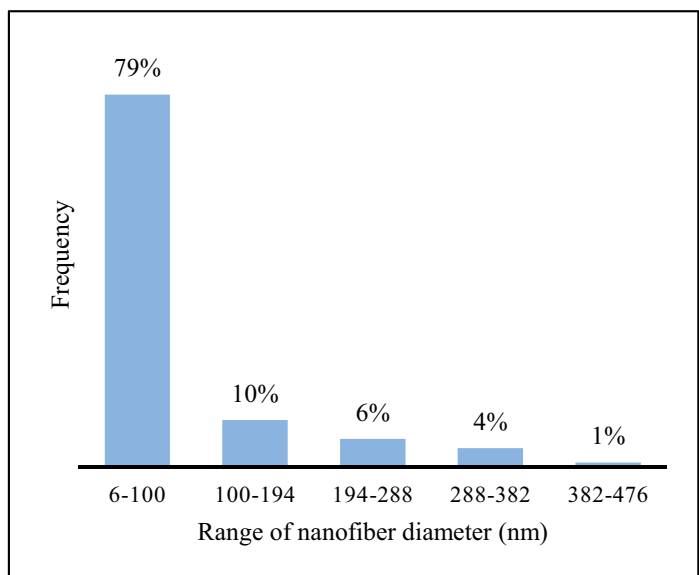
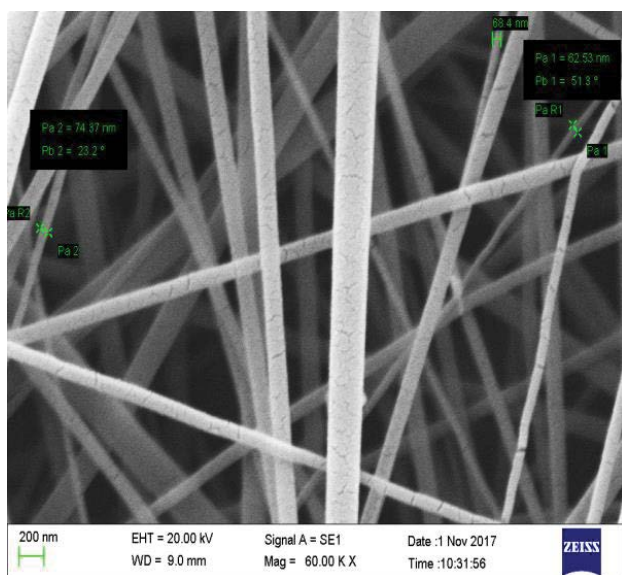


Fig. 4. SEM image and distribution diameter of PAN/Ahh.

Table 2
Calculated results for adsorption of Th⁴⁺ on PAN/Ahh

Experiment no.	pH	Th ⁴⁺ concentration (mg L ⁻¹)	Contact time (min)	Ahh conc. (wt%)	Ads (%)
1	6.5	32.5	35	42.5	99.1
2	6.5	32.5	65	42.5	98.0
3	5	55	50	55	93.6
4	5	55	50	5	86.5
5	3.5	32.5	35	42.5	97.1
6	3.5	32.5	35	17.5	93.0
7	6.5	77.5	65	17.5	87.6
8	5	100	50	30	85.1
9	3.5	32.5	65	42.5	93.5
10	5	55	50	30	98.2
11	3.5	32.5	65	17.5	87.4
12	3.5	77.5	35	42.5	89.2
13	6.5	77.5	35	17.5	89.7
14	5	55	20	30	99.1
15	5	55	50	30	97.2
16	8	55	50	30	85.2
17	5	10	50	30	95.6
18	6.5	32.5	35	17.5	96.1
19	5	55	50	30	97.0
20	5	55	50	30	98.2
21	3.5	77.5	35	17.5	92.3
22	5	55	50	30	97.0
23	5	55	50	30	97.1
24	5	55	80	30	98.2
25	6.5	77.5	65	42.5	90.7
26	6.5	77.5	35	42.5	88.8
27	2	55	50	30	84.8
28	6.5	32.5	65	17.5	89.4
29	3.5	77.5	65	17.5	90.3
30	3.5	77.5	65	42.5	90.7

Table 3
ANOVA results for the response: Th⁴⁺ removal

Source	Sum of square	df*	Mean square	F-value	p-value Prob. > F
Model	632.42	14	45.17	40.74	0.0001
Residual	16.63	15	1.11	–	–
Lack of fit	14.99	10	1.5	4.57	0.0538
Pure error	1.64	5	0.33	–	–
Total	649.06	29	–	–	–

$R^2 = 0.9744$, $R^2_{adj} = 0.9505$, $CV^{**} = 1.13\%$; * = degree of freedom; ** = coefficient of variation.

the large probability value (p -value) of lack of fit (0.0538) illustrate that the lack of fit was not significant; implying the model adequately described the data. In addition, the determination coefficient ($R^2 = 0.9744$) was reasonably practicable which described 97.44% of the total variation in the model.

Data must display homoscedasticity, which occurs when the variances of data accompanying the line of best-fit stay

similar to move along the line [37]. To check this assumption, the plot of studentized residuals versus the unstandardized predicted values were considered (Fig. 5). All points are uniformly dispersed around the line $e_i = 0$ without any specific trend which means data have homogeneity of variances.

The three dimensional (3-D) of the response surface and two dimensional (2-D) of the contour plots were considered in order to determine the optimum conditions of the adsorption

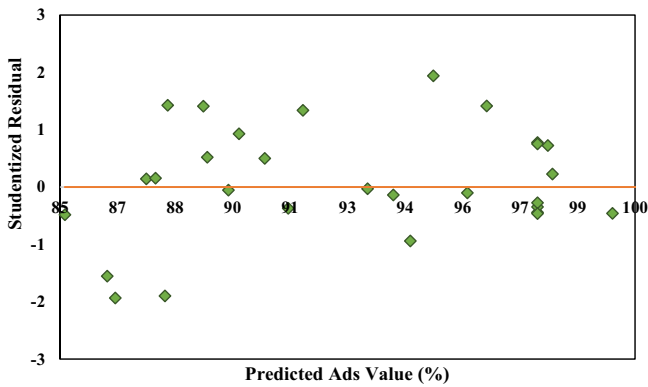


Fig. 5. Studentized residual plot for Ads(%) data versus the unstandardized predicted values.

process and visualize the correlation between the response (Ads%) and experimental levels of each variable (Figs. 6–8).

Figs. 6(a) and (b) depict the effect of contact time, which implied a considerable effect on removal percentage. Accordingly, when contact time was held below 42 min, about 95% removal was attained due to the plentiful availability of reaction sites regardless of Th⁴⁺ concentration, Ahh concentration, and pH. By increasing the contact time, the Th⁴⁺ ion adsorption decreased very slowly at about 60 min. The achievement of equilibrium adsorption might have been due to the reduction in the available active adsorption sites on the adsorbent with time resulting in limited mass transfer of the adsorbate molecules from the bulk liquid to the outer surface of PAN/Ahh.

Figs. 6(a), 7(a), and 8(a) show the combined effect of pH with contact time, Th⁴⁺ concentration, and Ahh concentration, respectively. Adsorption gained a maximum at a pH range 4.0–6.0 in all three figures regardless of Th⁴⁺ concentration, Ahh concentration, and contact time. The maximum

adsorption in the pH range 4.0–6.0 may be due to the formation of Th⁴⁺ complexes with carboxyl groups, owing to its consistency constant with Th⁴⁺ [38]. Accordingly, in strong acidic solution from pH 2.0 to 4.0 hydroxonium ions H₃O⁺ contend with the positive Th⁴⁺ ions for the adsorption sites and, the uncomplexed cation is unchanging at pH ≤ 3 [39].

The effects of Th⁴⁺ concentration are presented in Figs. 7(a) and (b). The extent of Ads% was decreased by approximately 4% when initial concentration was increased from 55 to 67 mg L⁻¹ for constant pH and contact time levels. On the contrary, the adsorption capacity of PAN/Ahh was calculated to increase with rise in initial concentration from 39 to 65 mg L⁻¹. This can mostly be attributed to the increase in concentration gradient in the system which consequences with enhanced efficiency of Th⁴⁺ adsorption.

Figs. 8(a) and (b) depict the influence of Ahh quantity in nanofiber adsorbent on metal ions adsorption. Accordingly, the adsorption capacity of Th⁴⁺ ion rises with an increase in Ahh amounts up to 40 wt%. This increment is due to the high dependence of the amine groups to interact with the Th⁴⁺ ions as well as the uniform surface and pore structure. Further increases in AMH quantities of more than 42 wt% cause a reduction in the adsorption capacity of the Th⁴⁺. This decrement can be due to a reduction in surface area and pore volume, which decreases the active sites of PAN/Ahh nanofibers for the adsorption process.

It was apparent that the first-order effects of Th⁴⁺ and Ahh concentration (*p*-value ≤ 0.05 and higher than *F* value) were more significant than the two other factors. The second-order main effects pH, Ahh, and Th⁴⁺ concentration (*p*-value_{pH}, *p*-value_{Ahh concentration}, and *p*-value_{Th concentration} ≤ 0.0001) were also highly significant as compared with the pH first-order main effects (*p*-value_{pH} ≤ 0.2169) for the Ads%. There was direct proportional relationship between pH and Th⁴⁺ concentration (*p*-value ≤ 0.0009) and the Ads% which was responsible for achieving a relatively higher Ads % predicted by the model and the response contour plot (Fig. 7(b)).

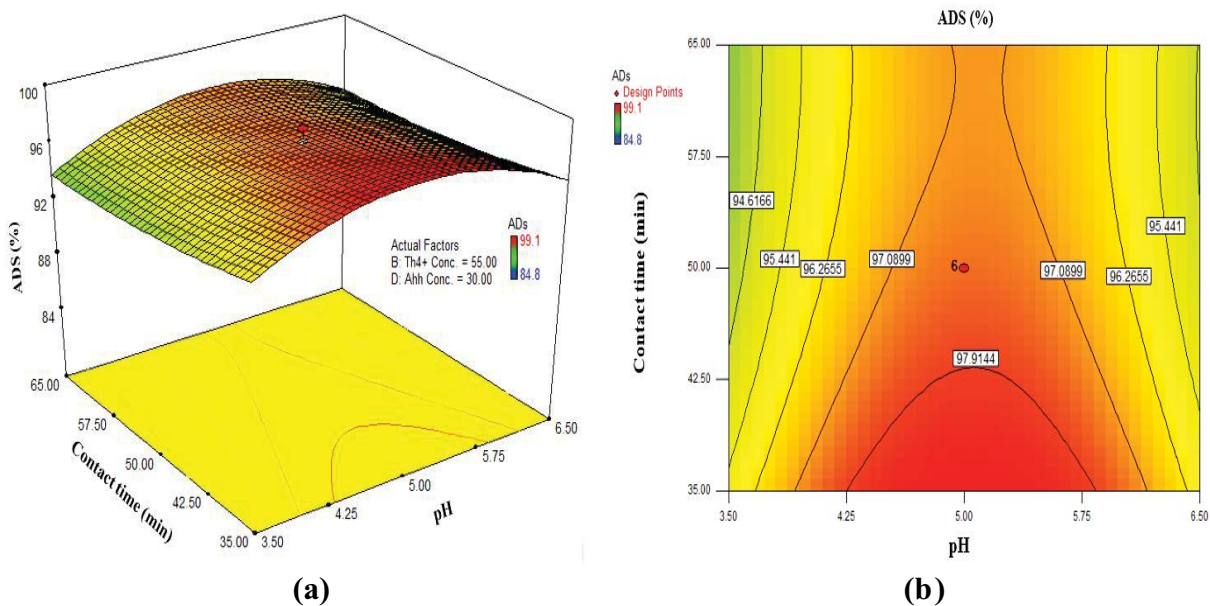


Fig. 6. (a) Surface, (b) contour plot for pH–contact time (Ahh concentration = 30; Th⁴⁺ concentration = 55 mg L⁻¹).

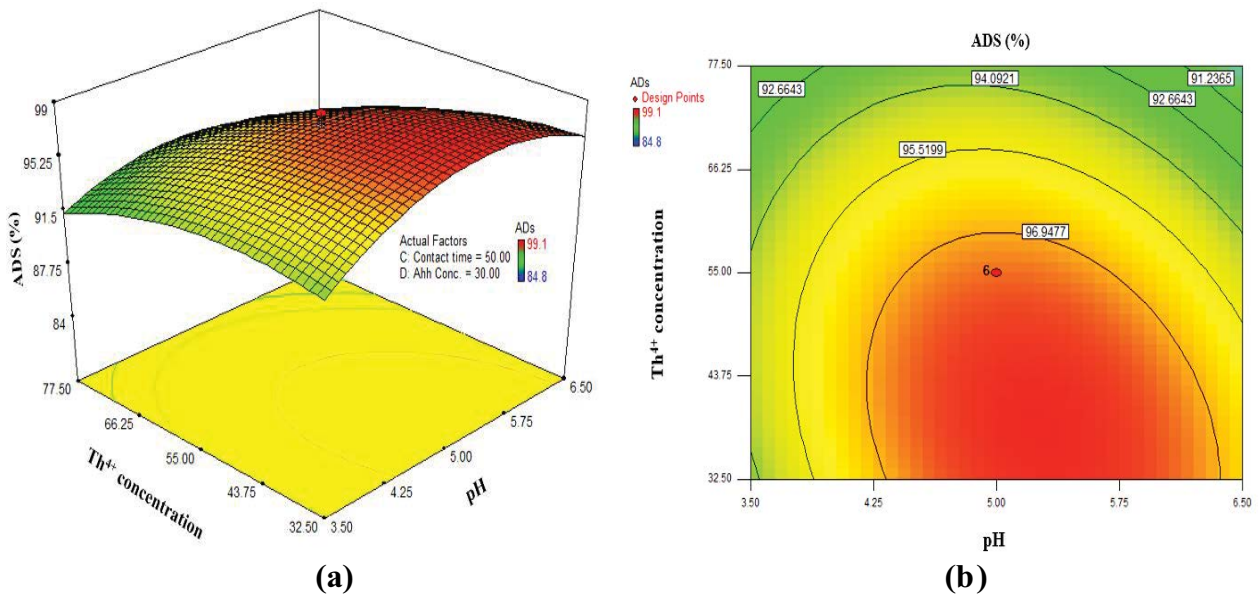


Fig. 7. (a) Surface, (b) contour plot for pH–Th⁴⁺ concentration (Ahh concentration = 30; contact time = 50 min).

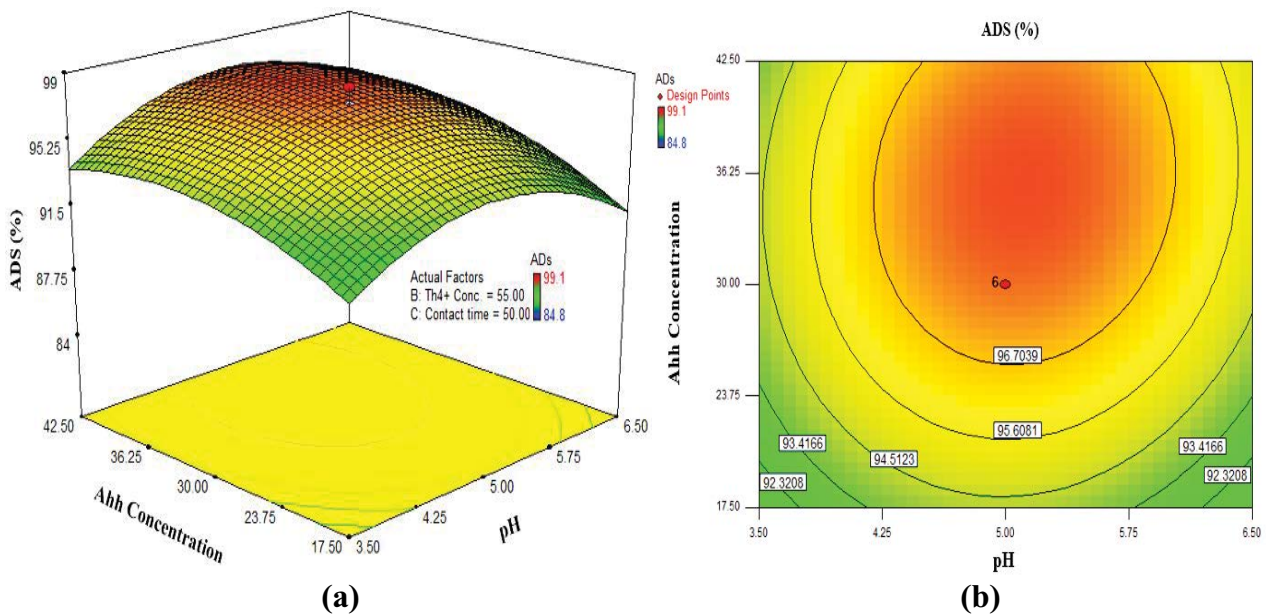


Fig. 8. (a) Surface, (b) contour plot for pH–Ahh concentration (Th⁴⁺ concentration = 55; contact time = 50 min).

3.3. Optimum conditions of adsorption process

Six optimum conditions were assumed by the design expert software in order to achieve the optimum conditions of the Ads%. Affirmative experiments were considered to investigate the correctness and validation of the optimum conditions. The results were compared with the output of the model (Table 4). It was observed that the maximum Ads (98.53%) achieved at 37.4 mg L⁻¹ of Th⁴⁺ concentration, pH = 5.3, Ahh concentration = 41 wt%, and 64.5 min contact time.

3.4. Kinetic analysis

In order to investigate the controlling mechanism of adsorption process of PAN/Ahh against Th⁴⁺, the pseudo-first and second-order models were considered to evaluate the experimental data obtained (Fig. 9).

Adsorption rate for PAN/Ahh is determined at various time under optimum adsorbent weight, contact time of 20–80 min, and optimal pH at temperature 25°C. Pseudo-first-order kinetic model indicates physical adsorption process while, the pseudo-second-order kinetic model specifies

Table 4
Comparison of predicted and observed values in optimum condition

NO.	pH	Th ⁴⁺ concentration (mg L ⁻¹)	Contact time (min)	Ahh concentration (mg L ⁻¹)	Ads (%)	
					Predicted	Observed
1	5.3	37.4	64.5	41.0	99.13	98.53
2	5.2	45.1	39.4	32.6	99.56	98.37
3	4.5	42.7	35.3	29.1	99.34	98.04
4	5.4	45.6	35.8	33.1	99.92	97.65
5	5.4	42.9	48.8	37.7	99.11	97.12
6	5.2	41.2	35.9	26.0	99.43	96.28

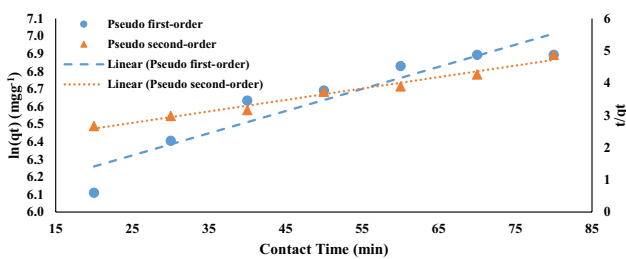


Fig. 9. Pseudo-first and second-order plots of Th⁴⁺ onto PAN/Ahh.

that the adsorption process is chemical and exchange of electrons happens between the adsorbent and the ion being adsorbed [40–42]. Eqs. (9) and (10) show the pseudo-first and second-order kinetic model, respectively:

$$q_t = q_e (1 - e^{-k_1 t}) \tag{9}$$

$$q_t = \frac{t q_e^2}{\frac{1}{k_2} + q_e t} \tag{10}$$

where q_e : amount of Th⁴⁺ uptake per unit mass of adsorbent at equilibrium (mg g⁻¹); q_t : amount of Th⁴⁺ uptake per unit mass of adsorbent at time t (mg g⁻¹); and k_1 and k_2 are reaction rate constants (mg g⁻¹ min⁻¹).

R^2 coefficient clearly indicates that Th⁴⁺ adsorption data on the PAN/Ahh have been best described by pseudo-second-order kinetic model, thus the rate-controlling step is chemical by complex formation/ion exchange (Table 5).

3.5. Adsorption isotherms

The purpose of adsorption isotherm calculation is to study the relationship between the quantity of adsorbent and

Table 5
Pseudo-first and second-order parameters

Kinetic model	Equation	q_e (mg g ⁻¹)	k_1 (min ⁻¹)	R^2
Pseudo-first order	0.013x + 6.007	406	0.013	0.88
Pseudo-second order	0.035x + 1.877	28	0.0268	0.98

the level of adsorption through the process [43]. Langmuir, Freundlich, and Dubinin–Radushkevich (D–R) isotherms were applied for analysis of adsorption equality (Figs. 10 and 11). The linearized form of the Langmuir equation which is used for monolayer adsorption on finite and similar surfaces is described by Eq. (11) as follows [44]:

$$\frac{C_e}{q_e} = \frac{1}{K_L q_m} + \frac{C_e}{q_m} \tag{11}$$

where q_m is the maximum monolayer adsorption capacity (mg g⁻¹); K_L is the Langmuir constant related to the free energy of adsorption (L mg⁻¹); and a plot of C_e/q_e versus C_e yields a straight line with slope $1/q_m$ and intercept $1/q_m K_L$.

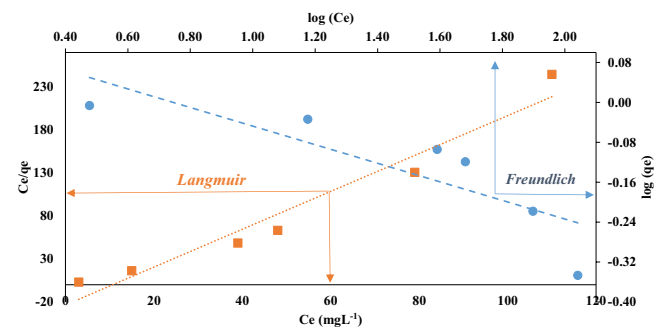


Fig. 10. Langmuir and Freundlich isotherms for adsorption of Th⁴⁺.

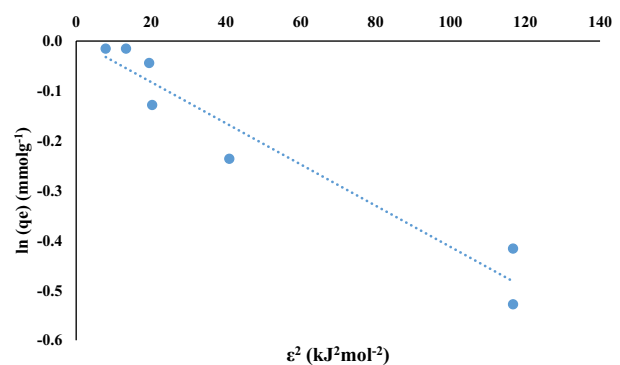


Fig. 11. Dubinin–Radushkevich (D–R) adsorption isotherm of Th⁴⁺ on PAN/Ahh.

The well-known form of the Freundlich isotherm is given by Eq. (12) as follows:

$$q_e = KfC_e^{1/n} \quad (12)$$

which after applying logarithm for both sides, converted into Eq. (13) as follows:

$$\log(q_e) = \log(Kf) + \frac{1}{n}\log(C_e) \quad (13)$$

where Kf and $\frac{1}{n}$ are the Freundlich constants related to the adsorption capacity and adsorption intensity, respectively.

Another popular isotherm model is D–R, which the nonlinear and linear forms of D–R are given by Eq. (14) as follows [45]:

$$q_e = q_{\max} e^{-K_{\text{ad}}\varepsilon^2} \quad (14)$$

which the linear form can be represented by Eq. (15) as follows:

$$\ln(q_e) = \ln(q_{\max} - K_{\text{ad}}\varepsilon^2) \quad (15)$$

where q_e is the amount of Th^{4+} (mmol g^{-1}) adsorbed per unit mass of PAN/Ahh, q_{\max} is the theoretical adsorption capacity (mmol g^{-1}), K_{ad} is the constant related to the adsorption energy ($\text{mol}^2 \text{kJ}^{-2}$), and ε is the Polanyi potential that is determined as Eq. (16) as follows:

$$\varepsilon = RT \ln\left(1 + \frac{1}{C_e}\right) \quad (16)$$

where C_e is the solution concentration at equilibrium (mol L^{-1}), R is the gas constant ($8.314 \text{ J mol}^{-1} \text{ K}^{-1}$), and T is the absolute temperature of the aqueous solution (K). The amount of K_{ad} was estimated from the slope of the plot of $\ln q_e$ versus ε^2 and q_{\max} is prepared from the intercept. As stated, K_{ad} is related to adsorption energy, so the mean free energy of adsorption (E) (kJ mol^{-1}), is calculated according to Eq. (17) as follows [46]:

$$E = \frac{1}{\sqrt{2K_{\text{ad}}}} \quad (17)$$

Table 7

Comparison between the maximum monolayer adsorption capacity (q_m , mg g^{-1}) of various adsorbents [26–28,33,50,51]

No.	Adsorbent	q_m (mg g^{-1})	Ion	References
1	Modified polyacrylonitrile composite nanofiber adsorbent	249.4	Th^{4+}	[28]
2	Modified polyacrylonitrile composite nanofiber adsorbent	193.1	U^{6+}	[28]
3	Amidoxime-modified polyacrylonitrile (PAN-oxime) nanofibers	263.45	Pb^{2+}	[26]
4	PAN– TiO_2 nanofiber adsorbent modified with aminopropyltriethoxysilane	250	Th^{4+}	[27]
5	CeO_2 nanofiber adsorbent functionalized with mercapto groups	272.3	Pb^{2+}	[51]
6	Aminated Polyacrylonitrile Fibers	76.112	Pb^{2+}	[33]
7	Ferroxane/polyacrylonitrile nanocomposite nanofibers adsorbent	357.14	Pb^{2+}	[50]
8	PAN/Ahh	499	Th^{4+}	This study

Table 6

Equilibrium isotherm parameters of sorption of Th^{4+} at 25°C

Isotherms		
Langmuir	Equation	$2.20x - 23.50$
	q_m (mg g^{-1}):	499
	k_L (L mg^{-1}):	8.5×10^{-5}
	R^2	0.95
Freundlich	Equation	$-0.19x + 0.14$
	Kf (mg g^{-1})	1.06
	n (g L^{-1})	-5.37
	R^2	0.70
Dubinin–Radushkevich	Equation	$-0.0041x + 0.0005$
	K_{ad} ($\text{mol}^2 \text{kJ}^{-2}$)	0.0044
	q_{\max} (mmol g^{-1})	1.04
	R^2	0.93

The value of E is very effective in determining the nature of adsorption. If the value is smaller than $8 \text{ (kJ mol}^{-1}\text{)}$, then the adsorption is physical in nature and if it is between 8 and $16 \text{ (kJ mol}^{-1}\text{)}$, then the adsorption is chemical with an exchange of ions [47–49]. The value of “ E ” was found to be between 8 and $16 \text{ (kJ mol}^{-1}\text{)}$, therefore the adsorption was chemical in nature for the PAN/Ahh, which is consistent with the results of Section 3.5.

The parameters calculated from the Langmuir, Freundlich, and D–R models are summarized in Table 6. The higher R^2 coefficients indicate that Langmuir model ($R^2 \geq 0.98$) fits the adsorption data best compared with the Freundlich and D–R model over the whole range of adsorptive concentration studied. According to Langmuir isotherm, maximum adsorption capacity was 430 mg g^{-1} at 25°C .

Table 7 presents the comparison between the maximum monolayer adsorption capacity (q_m , mg g^{-1}) of various PAN composites in the literature, which indicates the high efficiency of PAN/Ahh for Th^{4+} adsorption.

3.6. Thermodynamic studies

Enthalpy change (ΔH°), Gibbs free energy change (ΔG°), and entropy change (ΔS°) can be considered by employing equilibrium constants changing with temperature. The

Table 8
Thermodynamic parameters for adsorption of Th⁴⁺ by PAN/Ahh

Adsorbent	Temperature (K)	ΔG° (kJ mol ⁻¹)	ΔH° (kJ mol ⁻¹)	ΔS° (kJ K ⁻¹ mol ⁻¹)
PAN/Ahh	298	-86.8	81.87	291.54
	303	-88.3		
	308	-89.7		
	313	-91.2		
	318	-92.6		

distribution coefficient is relevant to the enthalpy change (ΔH°) and entropy change (ΔS°) at constant temperature (T^{-1}) by the rearrangement of the Van't Hoff Eq. (18) as follows:

$$\ln(K_d) = \frac{\Delta S^\circ}{R} - \frac{\Delta H^\circ}{RT} \quad (18)$$

where $\ln(K_d)$ is the distribution coefficient (mL g⁻¹); (ΔS°) standard entropy; (ΔH°) standard enthalpy; T , the absolute temperature (K); and R gas constant (kJ^omol⁻¹K⁻¹). The standard free energy value is calculated from Eq. (19) as follows:

$$\Delta G^\circ = \Delta H^\circ - T\Delta S^\circ \quad (19)$$

The experiments were carried out at five temperatures (25°C, 30°C, 35°C, 40°C, and 45°C), for solution concentration of 100 mg L⁻¹ of Th⁴⁺ (Fig. 12).

The values of ΔH° and ΔS° were calculated from the slopes and intercepts of linear regression of $\ln(K_d)$ versus T^{-1} ($R^2 > 0.99$). The results in Table 8 indicate that the process is endothermic and the adsorption capacity of the PAN/Ahh rises with temperature.

The positive values of $\Delta H^\circ > 0$ are indicative of an endothermic nature, which prefers the adsorption of Th⁴⁺ ion at the higher temperature [52]. In addition, the $\Delta S^\circ > 0$ is indicative of higher randomness of adsorption in the system and favors the stability of the adsorption. The negative values of $\Delta G^\circ < 0$ for these processes verify the probability and natural nature of adsorption process [53].

3.7. Desorption studies

The results regarding Th⁴⁺ ions desorbing percentage with various agents are shown in Table 9. The maximum

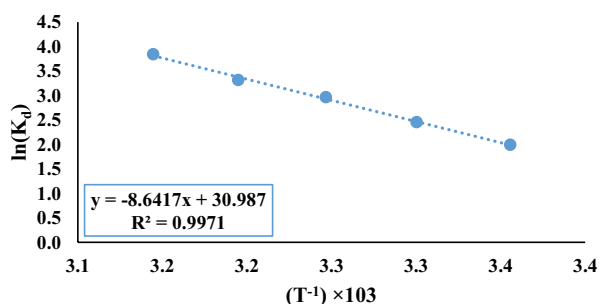


Fig. 12. Temperature dependence of the adsorption of Th⁴⁺ for PAN/Ahh.

Table 9
Desorption results in 0.1 M solution (%) on PAN/Ahh loaded with Th⁴⁺ ion

Agents	Desorption (%)
NaOH	53.94
NaCl	65.19
HCl	89.25
HNO ₃	92.69
NaOH/NaCl	68.63
HNO ₃ /HCl	94.5

Th⁴⁺ ions desorption level from the PAN/Ahh (94.5%) was obtained by using the 1 M HNO₃/1 M HCl solution. Similar results by using HNO₃/HCl solution but at different desorption level were reported in the literature [27]. After six cycles, the adsorption capacity of the PAN/Ahh decreased from 98.5% to 86%, while the recovery of Th⁴⁺ ion in HNO₃/HCl was reduced from 94.5% at first to 84.36% by the six times of usage.

4. Conclusion

In this study, PAN/Ahh adsorbent was prepared, characterized and a comprehensive investigation were carried out on its adsorption capacity for the removal of Th⁴⁺ ions from aqueous solution. Th⁴⁺ ion adsorption onto the PAN/Ahh was determined and optimized, namely the Ahh concentration, pH, Th⁴⁺ concentration, and contact time; using RSM. Accordingly, the maximum of 98.5% Th⁴⁺ removal was attained at Ahh concentration = 41 (wt%), pH 5.3, and 64.5 min contact time from a solution initially concentrated as 37.4 mg L⁻¹ Th⁴⁺ ions. The adsorption kinetics of Th⁴⁺ on the PAN/Ahh can be described by pseudo-second-order kinetic model, which indicates that adsorption involves chemical reaction. In addition, the Langmuir isotherm model correlated with the experimental data well. The adsorption process for PAN/Ahh was spontaneous ($\Delta G^\circ < 0$) and endothermic ($\Delta H^\circ > 0$) in nature.

The results showed the PAN/Ahh has a superior adsorption capacity for Th⁴⁺ ion (499 mg g⁻¹ at 25°C) when compared with other adsorbents reported in the literature. Consequently, results indicated the possibility of using the PAN/Ahh for efficient removal of Th⁴⁺ ion from aqueous solutions. Th⁴⁺ ion desorption studies revealed that Th⁴⁺ ions may be recovered to the extent of over 94.5% when using acidic desorbing agent (HNO₃/HCl solution).

Acknowledgment

This research was supported by Nuclear Science and Technology Research Institute of Iran; under project PRI-C5-93-001. The authors would like to thank the institute for providing assistance with analysis of samples carried out through this study.

References

- [1] S. Balasubramaniana, Chitosan-Based Polymer Nanocomposites for Heavy Metal Removal, Nanocomposites in Wastewater Treatment, Pan Stanford Publishing, Pte, Singapore, 2014.
- [2] D. Humelnicu, M.V. Dinu, E.S. Drăgan, Adsorption characteristics of UO_2^{2+} and Th^{4+} ions from simulated radioactive solutions onto chitosan/clinoptilolite sorbents, *J. Hazard. Mater.*, 185 (2011) 447–455.
- [3] V. Jain, R. Pandya, S. Pillai, P. Shrivastav, Simultaneous preconcentration of uranium (VI) and thorium (IV) from aqueous solutions using a chelating calix [4] arene anchored chloromethylated polystyrene solid phase, *Talanta*, 70 (2006) 257–266.
- [4] A. Nilchi, T.S. Dehaghan, S.R. Garmarodi, Kinetics, isotherm and thermodynamics for uranium and thorium ions adsorption from aqueous solutions by crystalline tin oxide nanoparticles, *Desalination*, 321 (2013) 67–71.
- [5] T.P. Rao, P. Metilda, J.M. Gladis, Preconcentration techniques for uranium (VI) and thorium (IV) prior to analytical determination—an overview, *Talanta*, 68 (2006) 1047–1064.
- [6] P. Vijayan, I. Dulera, P. Krishnani, K. Vaze, S. Basu, R. Sinha, Overview of the thorium programme in India, in: *Thorium Energy for the World*, Springer, 2016, pp. 59–69.
- [7] V. Höllriegel, M. Greiter, A. Giussani, U. Gerstmann, B. Michalke, P. Roth, U. Oeh, Observation of changes in urinary excretion of thorium in humans following ingestion of a therapeutic soil, *J. Environ. Radioact.*, 95 (2007) 149–160.
- [8] F.A. Aydin, M. Soylak, A novel multi-element coprecipitation technique for separation and enrichment of metal ions in environmental samples, *Talanta*, 73 (2007) 134–141.
- [9] W.H. Brattain, J.A. Becker, Thermionic and adsorption characteristics of thorium on tungsten, *Phys. Rev.*, 43 (1933) 428.
- [10] A. Jyothi, G. Rao, Solvent extraction behaviour of lanthanum (III), cerium (III), europium (III), thorium (IV) and uranium (VI) with 3-phenyl-4-benzoyl-5-isoxazolone, *Talanta*, 37 (1990) 431–433.
- [11] K.A. Kraus, G.E. Moore, F. Nelson, Anion-exchange studies. XXI. Th (IV) and U (IV) in hydrochloric acid. Separation of thorium, protactinium and uranium, *J. Am. Chem. Soc.*, 78 (1956) 2692–2695.
- [12] Z. Shiri-Yekta, M.R. Yaftian, A. Nilchi, Silica nanoparticles modified with a Schiff base ligand: an efficient adsorbent for Th (IV), U (VI) and Eu (III) ions, *Korean J. Chem. Eng.*, 30 (2013) 1644–1651.
- [13] C.W. Sill, C. Willis, Precipitation of submicrogram quantities of thorium by barium sulfate and application to the fluorometric determination of thorium in mineralogical and biological samples, *Anal. Chem.*, 36 (1964) 622–630.
- [14] M. Tsezos, B. Volesky, Biosorption of uranium and thorium, *Biotech. Bioeng.*, 23 (1981) 583–604.
- [15] D. Zhang, S. Wei, C. Kaila, X. Su, J. Wu, A.B. Karki, D.P. Young, Z. Guo, Carbon-stabilized iron nanoparticles for environmental remediation, *Nanoscale*, 2 (2010) 917–919.
- [16] T. Gäfvert, C. Ellmark, E. Holm, Removal of radionuclides at a waterworks, *J. Environ. Radioact.*, 63 (2002) 105–115.
- [17] Y. Chen, L. Zhao, Y. Wei, L.-F. He, F.-D. Tang, Adsorption characteristics of thorium on silica-based anion exchange resins, *Nucl. Sci. Technol.*, 26 (2015) 55–62.
- [18] D. Li, Y. Zuo, S. Meng, Separation of thorium (IV) and extracting rare earths from sulfuric and phosphoric acid solutions by solvent extraction method, *J. Alloys Compd.*, 374 (2004) 431–433.
- [19] S. Pollard, G. Fowler, C. Sollars, R. Perry, Low-cost adsorbents for waste and wastewater treatment: a review, *Sci. Total Environ.*, 116 (1992) 31–52.
- [20] A. Rahmati, A. Ghaemi, M. Samadfam, Kinetic and thermodynamic studies of uranium (VI) adsorption using Amberlite IRA-910 resin, *Ann. Nucl. Eng.*, 39 (2012) 42–48.
- [21] F.L. Zhou, R.H. Gong, Manufacturing technologies of polymeric nanofibres and nanofibre yarns, *Polym. Int.*, 57 (2008) 837–845.
- [22] D. Mohan, C.U. Pittman, Activated carbons and low cost adsorbents for remediation of tri- and hexavalent chromium from water, *J. Hazard. Mater.*, 137 (2006) 762–811.
- [23] M. Saifuddin, P. Kumaran, Removal of heavy metal from industrial wastewater using chitosan coated oil palm shell charcoal, *Elect. J. Biotechnol.*, 8 (2005) 43–53.
- [24] P. Kampalanonwat, P. Supaphol, Preparation and adsorption behavior of aminated electrospun polyacrylonitrile nanofiber mats for heavy metal ion removal, *ACS App. Mater. Interface*, 2 (2010) 3619–3627.
- [25] A. Nilchi, R. Saberi, S.R. Garmarodi, A. Bagheri, Evaluation of PAN-based manganese dioxide composite for the sorptive removal of cesium-137 from aqueous solutions, *Appl. Radiat. Isot.*, 70 (2012) 369–374.
- [26] K. Saeed, S. Haider, T.-J. Oh, S.-Y. Park, Preparation of amidoxime-modified polyacrylonitrile (PAN-oxime) nanofibers and their applications to metal ions adsorption, *J. Membr. Sci.*, 322 (2008) 400–405.
- [27] M. Mokhtari, A.R. Keshtkar, Removal of Th (IV), Ni (II) and Fe (II) from aqueous solutions by a novel PAN-TiO₂ nanofiber adsorbent modified with aminopropyltriethoxysilane, *Res. Chem. Intermed.*, 42 (2016) 4055–4076.
- [28] A. Dastbaz, A.R. Keshtkar, Adsorption of Th⁴⁺, U⁶⁺, Cd²⁺, and Ni²⁺ from aqueous solution by a novel modified polyacrylonitrile composite nanofiber adsorbent prepared by electrospinning, *Appl. Surf. Sci.*, 293 (2014) 336–344.
- [29] M. Douglas, *Design and Analysis of Experiments*, Wiley, UK, 2009.
- [30] T.K. Trinh, L.-S. Kang, Application of response surface method as an experimental design to optimize coagulation tests, *Environ. Eng. Res.*, 15 (2010) 63–70.
- [31] S. Lee, J. Kim, B.-C. Ku, J. Kim, H.-I. Joh, Structural evolution of polyacrylonitrile fibers in stabilization and carbonization, *Adv. Chem. Eng. Sci.*, 2 (2012) 275.
- [32] A. Ladhe, P. Frailie, D. Hua, M. Darsillo, D. Bhattacharyya, Thiol-functionalized silica-mixed matrix membranes for silver capture from aqueous solutions: experimental results and modeling, *J. Membr. Sci.*, 326 (2009) 460–471.
- [33] S. Deng, R. Bai, J.P. Chen, Aminated polyacrylonitrile fibers for lead and copper removal, *Langmuir*, 19 (2003) 5058–5064.
- [34] T.S. Anirudhan, S. Rijith, A.R. Tharun, Adsorptive removal of thorium (IV) from aqueous solutions using poly (methacrylic acid)-grafted chitosan/bentonite composite matrix: process design and equilibrium studies, *Colloids Surf., A*, 368 (2010) 13–22.
- [35] M. Talebi, S. Abbaszadeh, A.R. Keshtkar, Evaluation of single and simultaneous thorium and uranium sorption from water systems by an electrospun PVA/SA/PEO/HZSM5 nanofiber, *Process Saf. Environ. Prot.*, 109 (2017) 340–356.
- [36] M. Zulkali, A. Ahmad, N. Norulakmal, *Oryza sativa* L. husk as heavy metal adsorbent: optimization with lead as model solution, *Bioresour. Technol.*, 97 (2006) 21–25.
- [37] S. Azadi, A. Karimi-Jashni, S. Javadpour, Photocatalytic treatment of landfill leachate using W-doped TiO₂ nanoparticles, *J. Environ. Eng.*, 143 (2017) 04017049.
- [38] D. Langmuir, J.S. Herman, The mobility of thorium in natural waters at low temperatures, *Geochim. Cosmochim. Acta*, 44 (1980) 1753–1766.
- [39] S. Savvin, Analytical use of arsenazo III: determination of thorium, zirconium, uranium and rare earth elements, *Talanta*, 8 (1961) 673–685.
- [40] J.F. Corbett, Pseudo first-order kinetics, *J. Chem. Educ.*, 49 (1972) 663.
- [41] F.-C. Wu, R.-L. Tseng, S.-C. Huang, R.-S. Juang, Characteristics of pseudo-second-order kinetic model for liquid-phase adsorption: a mini-review, *Chem. Eng. J.*, 151 (2009) 1–9.
- [42] H. Yuh-Shan, Citation review of Lagergren kinetic rate equation on adsorption reactions, *Scientomet*, 59 (2004) 171–177.

- [43] B. Hameed, D. Mahmoud, A. Ahmad, Equilibrium modeling and kinetic studies on the adsorption of basic dye by a low-cost adsorbent: coconut (*Cocos nucifera*) bunch waste, *J. Hazard. Mater.*, 158 (2008) 65–72.
- [44] Y. Wu, S.-Y. Kim, D. Tozawa, T. Ito, T. Tada, K. Hitomi, E. Kuraoka, H. Yamazaki, K. Ishii, Equilibrium and kinetic studies of selective adsorption and separation for strontium using DtBuCH18C6 loaded resin, *J. Nucl. Sci. Technol.*, 49 (2012) 320–327.
- [45] E. Metwally, T. El-Zakla, R. Ayoub, Thermodynamics study for the sorption of ^{134}Cs and ^{60}Co radionuclides from aqueous solutions, *J. Nucl. Radiochem. Sci.*, 9 (2008) 1–6.
- [46] M. Ghasemi, M. Naushad, N. Ghasemi, Y. Khosravi-Fard, Adsorption of Pb (II) from aqueous solution using new adsorbents prepared from agricultural waste: adsorption isotherm and kinetic studies, *J. Ind. Eng. Chem.*, 20 (2014) 2193–2199.
- [47] M. Bozorgi, S. Abbasizadeh, F. Samani, S.E. Mousavi, Performance of synthesized cast and electrospun PVA/chitosan/ZnO-NH₂ nano-adsorbents in single and simultaneous adsorption of cadmium and nickel ions from wastewater, *Environ. Sci. Pollut. Res.*, (2018) 1–16.
- [48] A. Dada, A. Olalekan, A. Olatunya, O. Dada, Langmuir, Freundlich, Temkin and Dubinin–Radushkevich isotherms studies of equilibrium sorption of Zn^{2+} onto phosphoric acid modified rice husk, *IOSR, J. Appl. Chem.*, 3 (2012) 38–45.
- [49] M.M. Tehrani, S. Abbasizadeh, A. Alamdari, S.E. Mousavi, Prediction of simultaneous sorption of copper (II), cobalt (II) and zinc (II) contaminants from water systems by a novel multi-functionalized zirconia nanofiber, *Desal. Wat. Treat.*, 62 (2017) 403–417.
- [50] G. Moradi, F. Dabirian, P. Mohammadi, L. Rajabi, M. Babaei, N. Shiri, Electrospun fumarate ferroxane/polyacrylonitrile nanocomposite nanofibers adsorbent for lead removal from aqueous solution: characterization and process optimization by response surface methodology, *Chem. Eng. Res. Des.*, 129 (2018) 182–196.
- [51] S. Yari, S. Abbasizadeh, S.E. Mousavi, M.S. Moghaddam, A.Z. Moghaddam, Adsorption of Pb (II) and Cu (II) ions from aqueous solution by an electrospun CeO_2 nanofiber adsorbent functionalized with mercapto groups, *Process Saf. Environ. Prot.*, 94 (2015) 159–171.
- [52] Ü.H. Kaynar, M. Ayvacklı, Ü. Hiçsönmez, S.Ç. Kaynar, Removal of thorium (IV) ions from aqueous solution by a novel nanoporous ZnO: isotherms, kinetic and thermodynamic studies, *J. Environ. Radioact.*, 150 (2015) 145–151.
- [53] P. Ilaiyaraja, A.K.S. Deb, K. Sivasubramanian, D. Ponraju, B. Venkatraman, Adsorption of uranium from aqueous solution by PAMAM dendron functionalized styrene divinylbenzene, *J. Hazard. Mater.*, 250 (2013) 155–166.